Hindawi
Shock and Vibration
Volume 2021, Article ID 6641839, 10 pages
https://doi.org/10.1155/2021/6641839

Research Article

Numerical Investigation on Cavitation Suppression of Microchannel over a NACA0012 Hydrofoil

Zhouhao Shi,[1] **Zhanshan Xie**,[1,2] **Weidong Shi**,[1,2] **Qinghong Zhang**,[1] **and Lingwei Tan**[1,2]

[1]*School of Mechanical Engineering, Nantong University, Nantong 226019, China*
[2]*Institute of Fluid Machinery and Marine Engineering Equipment, Nantong 226019, China*

Correspondence should be addressed to Zhanshan Xie; xiezs@ntu.edu.cn and Weidong Shi; shiwd@ntu.edu.cn

Received 4 December 2020; Revised 28 January 2021; Accepted 16 March 2021; Published 30 March 2021

Academic Editor: Qiu Lemiao

To find a better method to suppress cavitation, a microchannel design connecting the internal low-pressure area with the outside is proposed for the first time in this paper; the method was adopted to replenish fluid in the interior of the low-pressure area to inhibit cavitation. Through numerical simulation, it is found that the size and position of microchannel have a certain influence on the cavitation inhibition. The results show that the generation and development of cavitation, under the same working conditions, can be effectively restrained by adopting appropriate microchannel ($x = 0.05$ c, $d = 6$ cm). Compared with the original hydrofoil, the scale of cavitation is reduced by nearly 50%, and its turbulent kinetic energy remains unchanged. Therefore, it is considered that microchannel technology, as a new means of cavitation suppression, is of great significance to other types of fluid machinery.

1. Introduction

Cavitation has always been a difficult problem restricting the development of fluid machinery [1], although scholars and engineers had carried out many measures such as optimizing the structural parameters of runners or hydrofoil and adding inducers and other measures to restrain cavitation. For instance, Wu and Xiong [2] set arched protrusions on the suction surface of hydrofoil for blade head flow control, verifying the inhibitory effect of hindering backflow on cloudy cavitation. Singh et al. and Wang [3, 4] carried out experiments and numerical simulations of the flow around the hydrofoil and obtained the general characteristics of cloudy cavitation. Cheng [5] researched the effects of Mekle model and Schnerr and Sauer model to simulate the velocity field, streamline, and cavitation and then found that the Schnerr cavitation model is in good agreement with the experimental results. Wang [6] used the gap at the head of the hydrofoil to introduce the fluid from the pressure surface to the suction surface, which effectively suppressed the cavitation. Chen et al. [7, 8] found that the impeller with slot drainage has good anticavitation characteristics and can improve the hydraulic efficiency of the impeller. Although scholars have researched the cavitation suppression of pump [9, 10], hydrofoil [11–15], and other fluid machinery [16–19], they are still unable to deal with the cavitation problem caused by random cases. In order to solve the cavitation problem of hydrofoil or impeller caused by random cases, in this paper, the authors have selected the NACA0012 hydrofoil as the research object and researched the cavitation characteristics of the hydrofoil with different parameters and positions of the microchannel by using the Schnerr–Sauer cavitation model [20] and the k-ε turbulence model. Besides, the authors constructed microchannel in areas prone to cavitation and explored the suppression effect of local microchannel with different parameter structures on control hydrofoils. The research strategy is of great significance for the suppression of random cavitation.

2. NACA0012 Model

2.1. Geometrical Model. NACA0012 hydrofoil is selected as the research object of simulation, and we constructed a microchannel on the hydrofoil to adjust the pressure in cavitation zone. Then, in order to research the flow field characteristics of the NACA0012 hydrofoil during

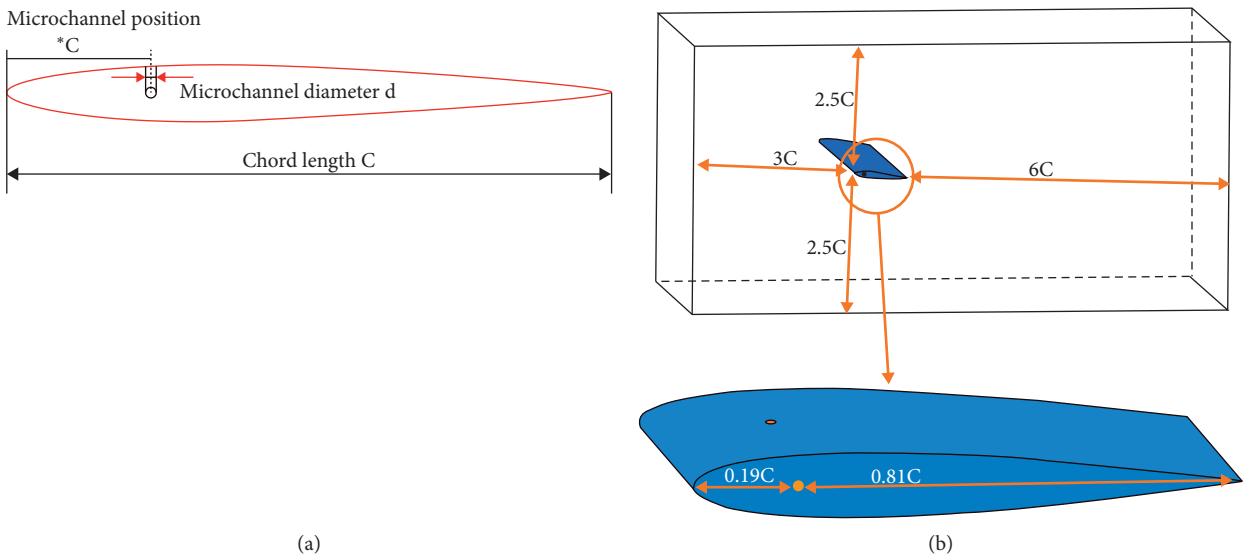

Figure 1: Geometrical model. (a) Structural dimension diagram. (b) Schematic diagram of NACA0012 computing domain.

cavitation, the structural dimensions of the hydrofoil and microchannel are shown in Figure 1(a), and the calculation domain selected is shown in Figure 1(b); the hydrofoil is located in the center of the upper and lower boundary, the hydrofoil is 3 c away from the inlet edge, the upper and lower boundary is 2.5 c, and the outlet edge is 6 c from the trailing edge. The geometric parameters of the foil are as follows: the chord length is 1 m, and the angle of attack of the incoming flow $\alpha = 6^{\circ}$.

2.2. Mesh Generation. The quality and quantity of the mesh have a great influence on the calculation results, so the structured mesh was used in the hydrofoil calculation domain, and the mesh around the foil was encrypted. Besides, the cavitation number of the hydrofoil is calculated according to formula (1), and the grid-independent analysis is carried out according to the cavitation number.

$$\sigma = \frac{p_{\infty} - p_v}{0.5\rho U^2}. \tag{1}$$

In the form, p_{∞} is the inlet pressure, saturated vapor pressure $p_v = 3540\ \mathrm{P_a}$, and U is the velocity of incoming flow at infinity. Therefore, when the boundary conditions are not changed, the cavitation number will not change; the following results are compared in the same cavitation number.

In order to ensure the dimensionless Yplus value of the wall function, the area near the wall and the wake area of the hydrofoil were locally encrypted, as shown in Figure 2(a). Finally, the mesh number of the model is determined to be 1.2 million.

2.3. Boundary Condition. The boundary condition is set as speed inlet and pressure outlet, and the microchannel adopts pressure inlet. The diameter and location of the microchannel in the cavitation area of the hydrofoil are shown in Table 1. In order to facilitate the analysis of different working conditions, the naming rule of the microchannel foil is as follows: the location of the microchannel to the size of the channel. The microchannel is set at 0.20 c in Figure 1, and the diameter of the microchannel is 4 mm, which is recorded here as 20~4.

3. Cavitation Model

Referring to literature [21, 22] and other related research results, the Schnerr–Sauer cavitation model can accurately simulate the state of cavitation. Therefore, this cavitation model is adopted in this paper. The growth and collapse of bubble clusters in the model are based on bubble dynamics of Rayleigh and Plesset.

$$\dot{m}^{-} = \frac{\rho_1\rho_v}{\rho_m}\frac{3\alpha_v(1-\alpha_v)}{R_B}\sqrt{\frac{2}{3}\frac{(p_v - p)}{\rho_m}}, \tag{2}$$

$$\dot{m}^{+} = -\frac{\rho_1\rho_v}{\rho_m}\frac{3\alpha_v(1-\alpha_v)}{R_B}\sqrt{\frac{2}{3}\frac{(p - p_v)}{\rho_m}}, \tag{3}$$

where R_B is the bubble radius, α_v is the volume fraction of the gas phase, and ρ_m, ρ_1, and ρ_v are the densities of mixed phase, liquid phase, and gas phase, respectively.

4. Result Analysis

4.1. Analysis of Cavitation Characteristics of Hydrofoil. Cavitation nephogram of NACA hydrofoil without microchannel is shown in Figure 3. It is obvious that cavitation occurs in the upper part of the hydrofoil, starting from the upper near-wall area 0.05 c away from the front end of the hydrofoil and continuing to the tail of the hydrofoil. The total length from the beginning of cavitation region to the tail is about 1.1 c, and it is about half as thick as the hydrofoil.

Due to the large cavitation distribution area of the original hydrofoil, firstly, at the initial cavitation distance of 0.05 c from the head, the microchannel apertures are set to be 2 mm, 4 mm, and 6 mm, respectively, and the cavitation

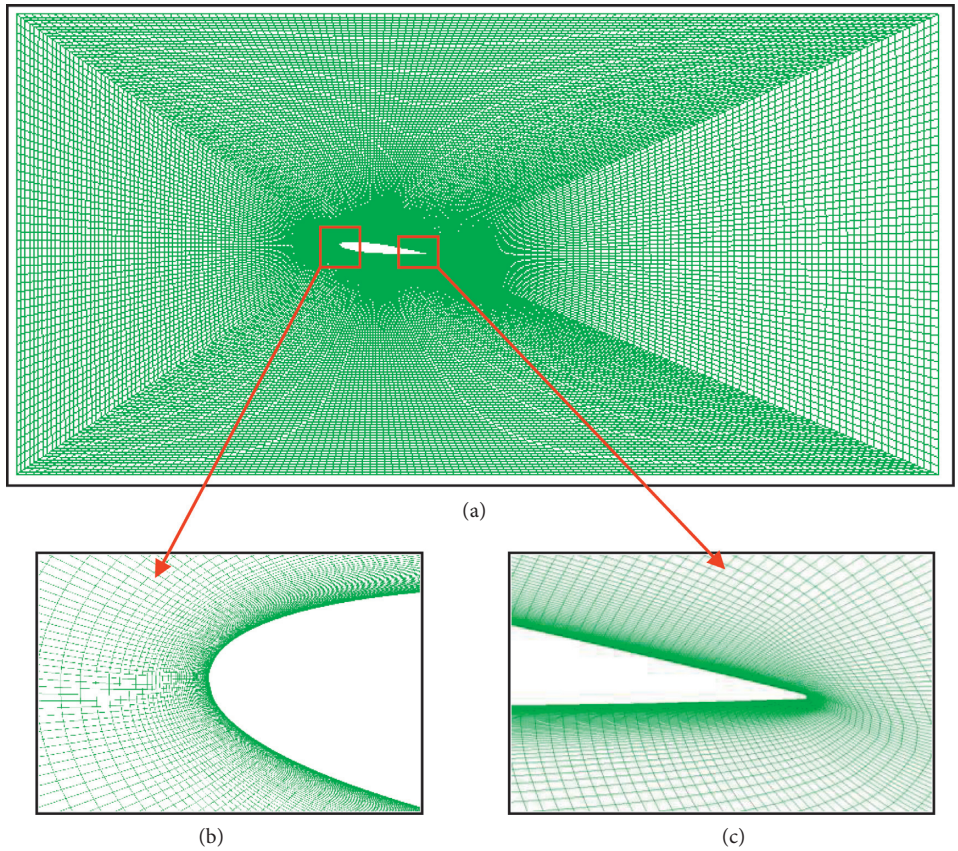

Figure 2: Computing mesh and mesh encryption around the foil. (a) Computational mesh. (b) Mesh encryption around the foil (head). (c) Mesh encryption at around the foil (tail).

Table 1: Solving working conditions.

Case	Microchannel position	d (mm)
1~3	0.05 c	2, 4, 6
4~5	0.1 c	2, 4
6~7	0.15 c	2, 4
8~9	0.2 c	2, 4
10	None	None

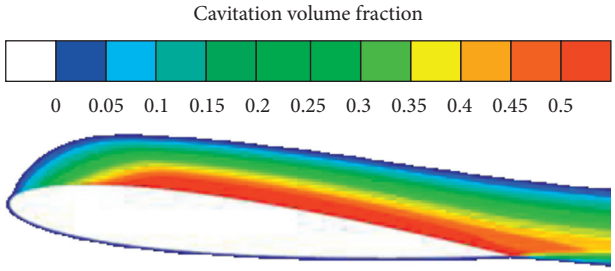

Figure 3: Cavitation nephogram without the influence of microchannel.

nephogram is shown in Figures 4(a)–4(c). By comparing the nephogram with the cavitation nephogram of hydrofoil without microchannel, it can be seen that "5~" series microchannels have well suppressed the scale of cavitation, and the inhibition effect of "5~2" and "5~6" microchannel is outstanding. Although the inhibition effect of 5~4 is worse than that of 5~2 and 5~6, it still keeps cavitation bubbles away from the near-wall surface and reduces the erosion damage of cavitation bubbles to the near-wall surface of hydrofoil to some extent. As for the cavitation suppression effect of "10~2" and "10~4" microchannels, compared with the hydrofoil without microchannel, the cavitation scale is also better suppressed. Although there is a relatively large cavitation area in "10~2," the cavitation area has been far away from the near-wall surface of NACA hydrofoil. This arrangement of microchannel is superior to the arrangement of "5~" series microchannel. However, the arrangement of "15~" and "20~" series of microchannel, with the same scale, cannot observe the local low-pressure area, which fully shows that these two kinds of microchannel can well inhibit cavitation and protect the hydrofoil from cavitation damage to a certain extent. Although the "10~4" hydrofoil has good cavitation suppression performance, the vortex near the wall needs to be further clarified. Therefore, the velocity vector and the flow field near the wall in Figure 4(e) are properly amplified (as shown in Figure 5). It is easy to know that there is an obvious vortex in the downstream area of the microchannel, and the center of the vortex deviates from the wall.

To observe the fine cavitation distribution in detail, the scale values of the nephogram scales in Figures 4(f)~4(i) are adjusted, and the fine cavitation distribution is shown

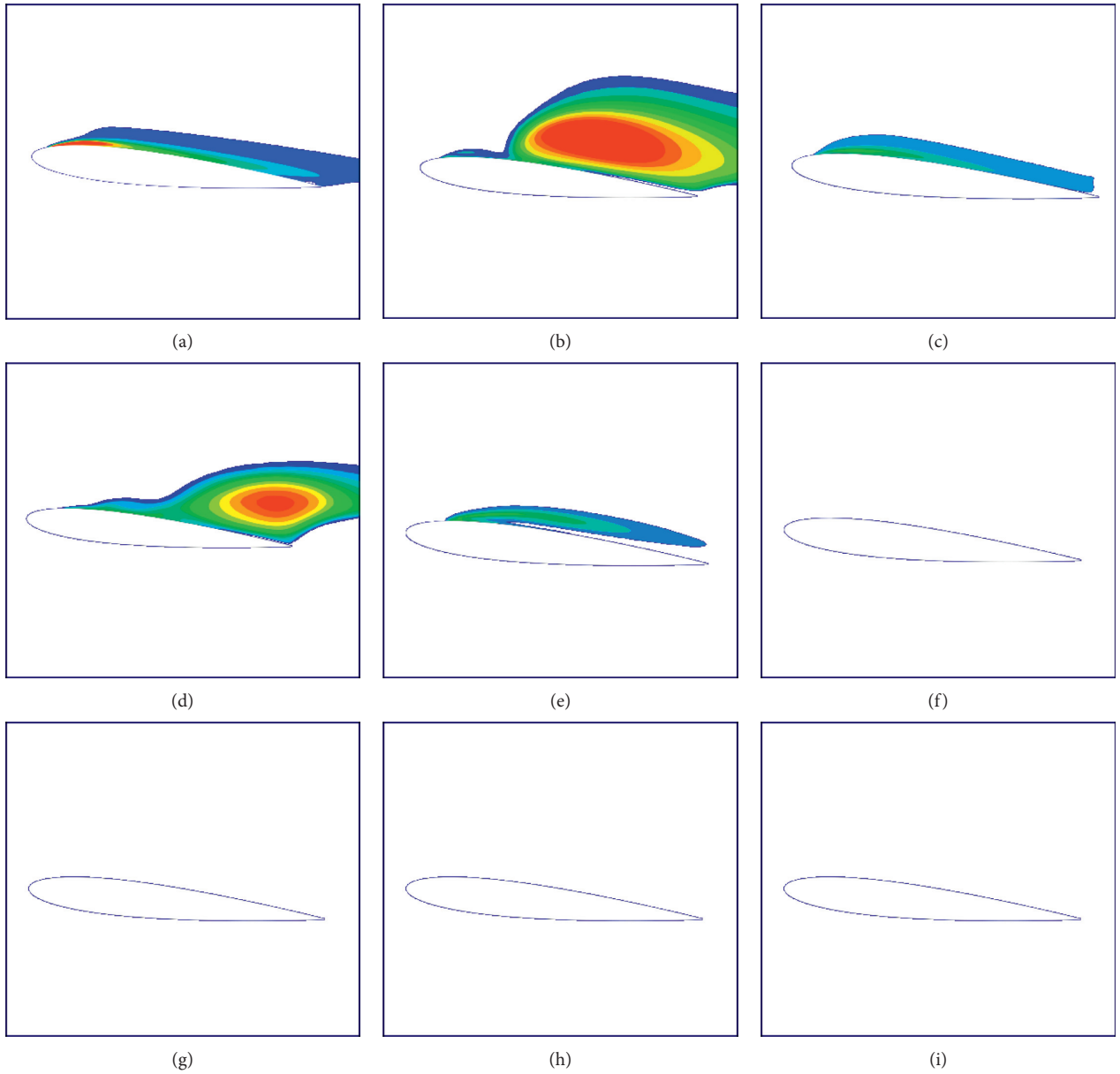

Figure 4: Cavitation nephogram of NACA hydrofoil. (a) 5~2 cavitation nephogram. (b) 5~4 cavitation nephogram. (c) 5~6 cavitation nephogram. (d) 10~2 cavitation nephogram. (e) 10~4 cavitation nephogram. (f) 15~2 cavitation nephogram. (g) 15~4 cavitation nephogram. (h) 20~2 cavitation nephogram. (i) 20~4 cavitation nephogram.

in Figure 6. It can be seen from Figure 6 that the area of "15~" cavitation is located at the tail of the hydrofoil, and the distribution area is small. The cavitation area of "20~" series hydrofoil can be considered to disappear completely. In other words, cavitation has been completely suppressed.

It can be seen that the cavitation suppression effect is remarkable when pressure regulating microchannel is set at and after 0.15 c, no matter the aperture is 2 mm or 4 mm. Compared with the simulation of the flow field around the original hydrofoil, the flow field of the hydrofoil with microchannel (2 mm, 4 mm, and 6 mm) at 0.05 c and 0.1 c positions has a better suppression of cavitation scale and keeps the cavitation area away from the near wall.

4.2. Analysis of Pressure Variation near the Wall of Hydrofoil. This section takes the coordinates and pressure points of several points in the upper part of the hydrofoil and compares them, and the curve (as shown Figure 7) shows the surface pressure changes of different microchannel diameters at different positions of 0.05 c, 0.1 c, 0.15 c, and 0.2 c from the hydrofoil head.

In Figure 7, the curve 0-0 is the control group, and the primitive hydrofoil is a low-pressure area at the position 0.05 c–0.3 c, and the pressure increases slowly after the position 0.3 c, while the hydrofoil pressure drops rapidly before the position 0.05 c, and 0.05 c–0.3 c is the cavitation primary part, which is consistent with the cavitation nephogram. As shown in Figure 7(a), the pressure near the wall of the "5~4" hydrofoil fluctuates greatly in different

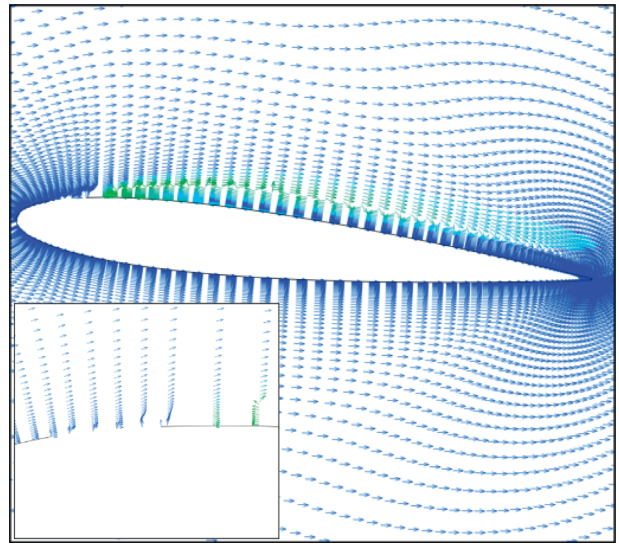

Figure 5: "10~4" velocity vector nephogram.

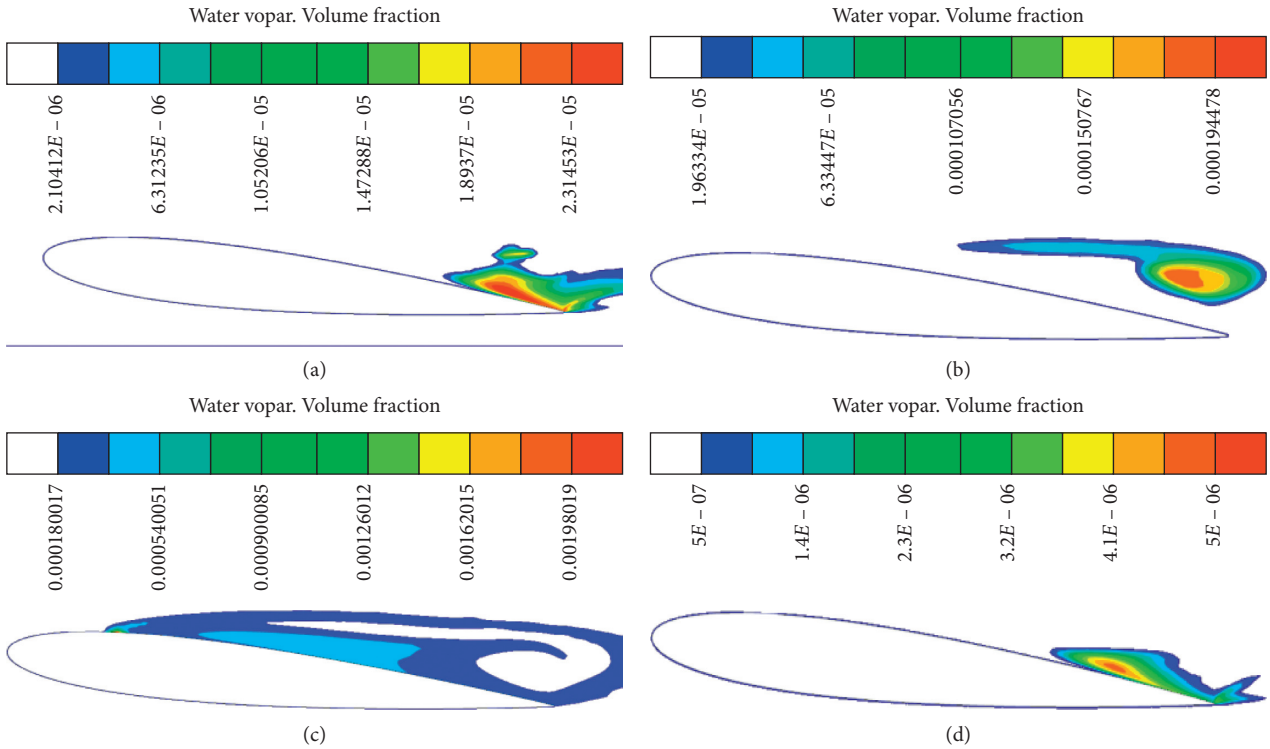

Figure 6: (a) 15~2 cavitation nephogram. (b) 15~4 cavitation nephogram. (c) 20~2 cavitation nephogram. (d) 20~4 cavitation nephogram.

positions, compared with the pressure near the wall of the hydrofoil without microchannel. Besides, the pressure near the wall of the airfoil is lower than that of the primitive hydrofoil at about 0.35 c. The pressure fluctuations of "5~2" and "5~6" basically coincide with the variation trend of "0~0" hydrofoil, especially since the pressure variation trend near the wall of "5~6" hydrofoil is very close to the variation trend of "0~0" hydrofoil.

For Figure 7(b), "10~4" hydrofoil has the same trend between 0.15 c and 0.3 c and has the same trend after 0.3 c. Compared with "0~0" hydrofoil near-wall pressure, the near-wall pressure of "10~2" hydrofoil has a similar change trend before 0.05 c, then it shows a fluctuating trend, and then drops rapidly after 0.6 c. In Figure 7(c), the pressure near the wall of "15~4" and "15~2" hydrofoil is quite different only at 0.1 c, and the pressure variation trend of other parts is similar, but the pressure variation trend near the wall of both hydrofoils is quite different from that of "0~0" hydrofoil. In Figure 7(d), "20~4" and "20~2" hydrofoils have the same pressure variation trend after 0.3 c, but there is a big

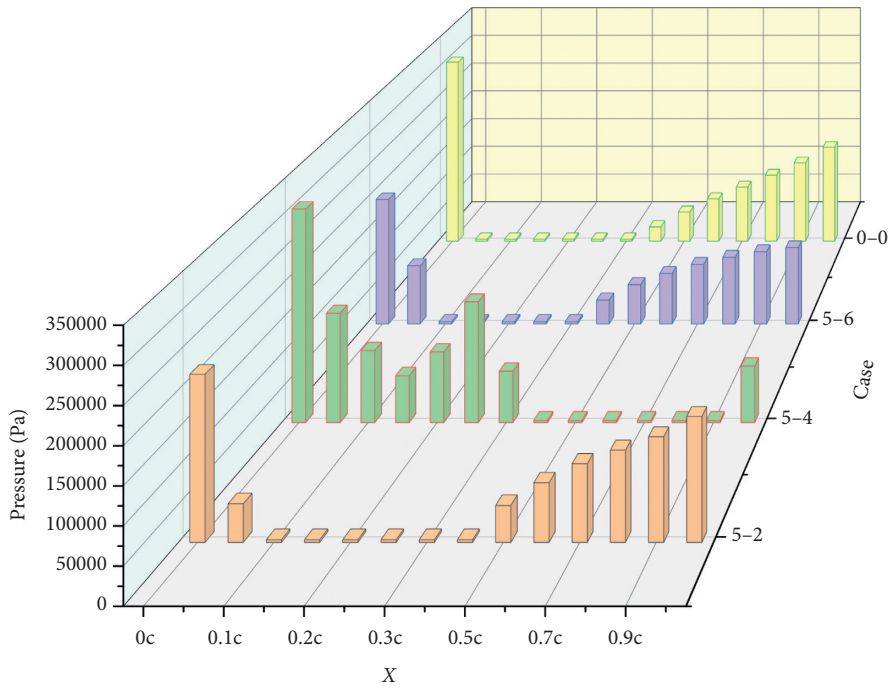

(a)

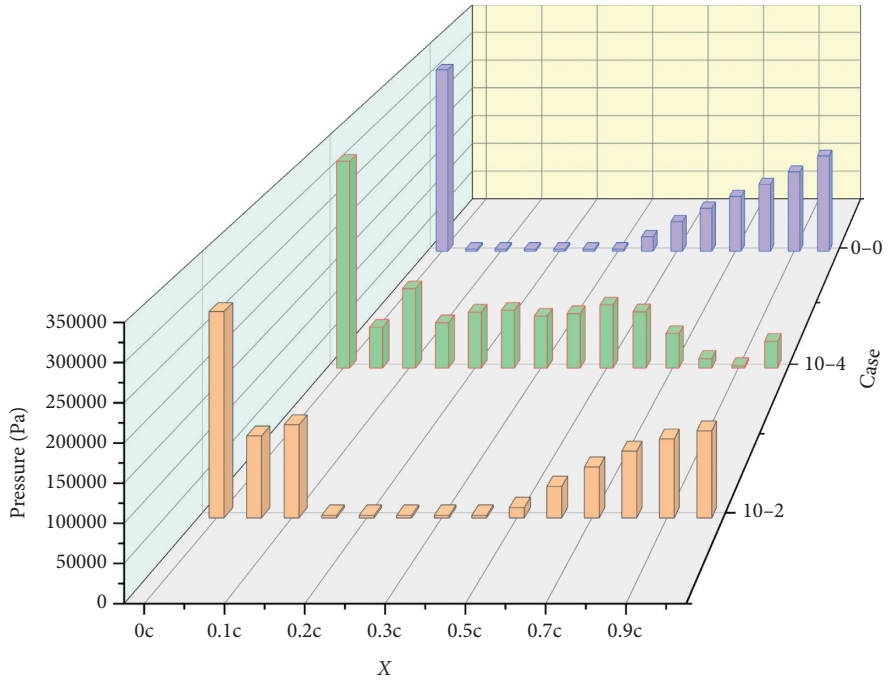

(b)

Figure 7: Continued.

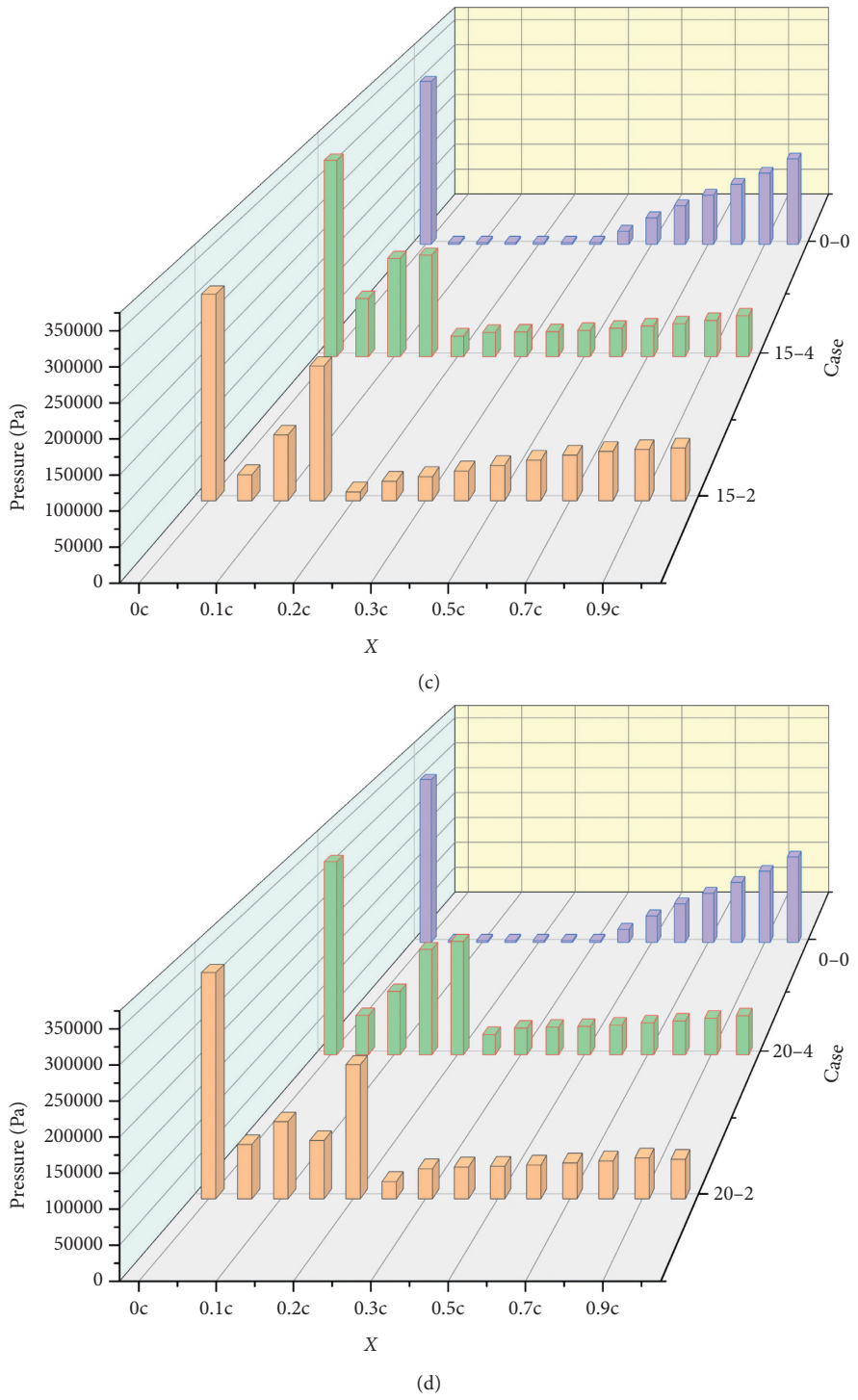

Figure 7: Pressure graph. (a) Near-wall pressure curve of "5~" series hydrofoil. (b) Near-wall pressure curve of "10~" series hydrofoil. (c) Near-wall pressure curve of "15~" series hydrofoil. (d) Near-wall pressure curve of "20~" series hydrofoil.

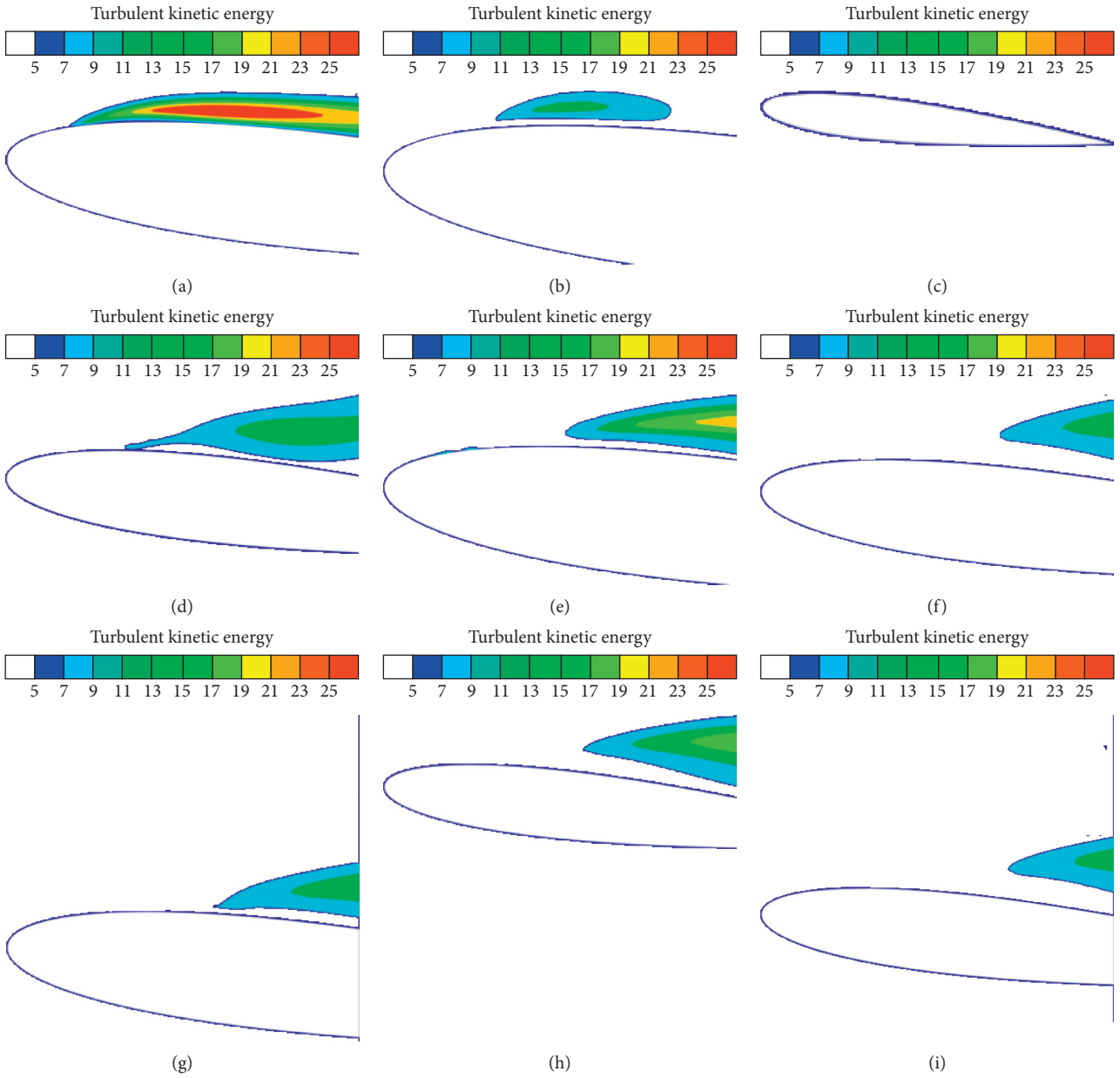

Figure 8: Turbulent kinetic energy nephogram of NACA hydrofoil with microchannel. (a) 5~2 turbulent kinetic energy nephogram. (b) 5~4 turbulent kinetic energy nephogram. (c) 5~6 turbulent kinetic energy nephogram. (d) 10~2 turbulent kinetic energy nephogram. (e) 10~4 turbulent kinetic energy nephogram. (f) 15~2 turbulent kinetic energy nephogram. (g) 15~4 turbulent kinetic energy nephogram. (h) 20~2 turbulent kinetic energy nephogram. (i) 20~4 turbulent kinetic energy nephogram.

Table 2: The factors and levels of the orthogonal test.

Parameters	Value
Inflow velocity	15 m/s, 20 m/s
Pressure in microchannel	0.5 atm, 1 atm, 1.5 atm, 2 atm
Number of microchannels	Single, multiple

difference between 0.25 c–0.05 c. Then, the trend of near-wall pressure is the same before 0.05 c.

To sum up, only from the effect of suppressing cavitation, the hydrofoil of microchannel "15~" and "20~" can restrain cavitation nearly 100%, and the hydrofoil of microchannel "5~" and "10~" series can also restrain the scale very well. From the point of view of structural cavitation damage, microchannel can prevent large-scale damage to the near wall of the hydrofoil to a certain extent. From the angle of flow field structure and turbulent kinetic energy of the hydrofoil, the microchannel "5~6" hydrofoil can well suppress cavitation and its hydrodynamic characteristics.

4.3. Turbulent Kinetic Energy Analysis of Hydrofoil. Turbulence is a kind of nonlinear fluid motion which is irregular in space and irregular in time. This kind of motion

Table 3: Test results and visual analysis report.

Test number	Pressure in microchannel	Inflow velocity	Number of microchannels	Cavitation	Pressure	Flow field	Average score
1	0.5	15	Single	0.9	0.8	1	0.90
2	0.5	20	Multiple	0.5	0.5	1	0.67
3	1	15	Single	0.8	0.9	0.9	0.87
4	1	20	Multiple	0.6	0.9	0.7	0.73
5	1.5	15	Multiple	1	1	0.9	0.97
6	1.5	20	Single	0.6	0.6	0.5	0.57
7	2	15	Multiple	1	1	0.2	0.73
8	2	20	Single	0.4	0.4	0.4	0.40
k1	0.78	0.87	0.68				
k2	0.80	0.59	0.76				
k3	0.77						
k4	0.57						
Range	0.23	0.28	0.08				

shows a highly complex three-dimensional unsteady and irregular flow state with rotation [23, 24]. Because of the complexity of turbulence, the concepts of turbulent kinetic energy and turbulent kinetic energy dissipation are derived. The turbulent kinetic energy is an important index to measure the fluid energy loss. The larger the turbulent kinetic energy is, the more complex the flow is and the more intense the energy exchange is.

According to the turbulent kinetic energy nephogram of hydrofoil (Figure 8), the turbulent kinetic energy of hydrofoil with "5~6" microchannel is less than that of hydrofoil without microchannel. In terms of suppressing the cavitation scale and the hydrodynamic characteristics of the hydrofoil, the hydrofoil with "5~6" microchannel can well meet the economic and safety performance. The turbulent kinetic energy of another microchannel hydrofoil is larger than that of hydrofoil without microchannels. From the perspective of energy capture, these microchannels reduce the economic benefits of hydrofoil.

5. Orthogonal Test and Result Analysis

In addition to researching the position and diameter of microchannel, the velocity of flow, pressure, and the number of microchannel are also the factors to inhibit cavitation. Therefore, the simulation research is carried out by using the method of orthogonal experiment to find the primary and secondary order of the influence of microchannel layout parameters on cavitation suppression. The factors and levels of the orthogonal test are shown in Table 2, and the interactions among the factors which are marked as A, B, and C, respectively, are ignored for the time being. Besides, due to the different levels of various factors, the mixed horizontal orthogonal experimental design is adopted, and the mixed horizontal orthogonal table L8 ($4^1 \times 2^4$) is selected, and the results are analyzed intuitively.

To facilitate the comparison of numerical results, the result will be converted into a value of 0-1 by quantifying the cloud picture of the result for measurement and comparison, and the arithmetic mean of each item will be taken as the final evaluation standard. The results are shown in Table 3.

It can be seen from Table 3 that the primary and secondary order of the influence of various parameters on cavitation is inflow velocity > pressure in microchannel > number of microchannel. Cavitation number directly determines the main factor of the intensity of cavitation. And the main artificially controllable factor of using local microchannel to inhibit cavitation is pressure in microchannel, whose merit value is between 0.5 and 1.5 standard atmospheric pressure, and its value falling outside the range of merit value will obviously weaken or even aggravate cavitation, and the inhibition effect of porous is better than that of single hole.

6. Conclusion

(1) The hydrofoil with microchannels can significantly inhibit the existence of upper low-pressure area and eliminate the environment in which cavitation occurs. Then, microchannels at different positions have different inhibitory effects on cavitation; in terms of cavitation suppression, the microchannel at 0.15 c–0.2 c can completely suppress cavitation, and the cavitation at 0.05 c–0.1 c can also suppress more than 50% compared with the original hydrofoil.

(2) The pressure distribution on the upper side of the airfoil is obviously affected by the microchannel. The inflow of two different velocities leads to vortex on the side of the microchannel, and these vortices will cause vortex cavitation, which is the reason for the intensification of cavitation in 5-2 and 10-4.

(3) When the fluid collides in the microchannel region, the increase of turbulent kinetic energy and turbulent kinetic energy dissipation leads to the change of the lift-drag ratio of the hydrofoil. However, the turbulence intensity of "5~6" hydrofoil is the weakest, which has little effect on the mechanical performance.

(4) The research on the primary and secondary factors affecting airfoil cavitation shows that the operating condition is the most important factor affecting airfoil cavitation. The merit value of microchannel outlet pressure is 0.5–1.5 atmospheric pressure, which falls outside the range of merit value, which

will weaken the inhibition effect and even aggravate the cavitation. Microchannel outlet holes and holes can influence each other to enhance the effect of inhibiting cavitation.

Data Availability

Some or all data, models, or codes generated or used during the study are available from the corresponding author upon request.

Conflicts of Interest

The authors declare that they have no conflicts of interest.

Acknowledgments

The authors acknowledge the financial support from the National Natural Science Foundation of China (no. 51579118), National Key R&D Plan (2019YFB2005300), National High-Tech Ship Research Project (Ministry of Industry and Information Technology [2019], no. 360), Nantong University (no. 19R86), and Water Conservancy Science and Technology Project of Jiangsu Province (no. 2019038).

References

[1] Z. Xie, W. Shi, Y. Zheng et al., "Simulation investigation on impact damage characteristics of metal plate by cavitating bubble micro-jet water hammer," *Engineering Failure Analysis*, vol. 115, Article ID 104626, 2020.

[2] W. Wu and Y. Xiong, "A modified design method of anti-cavitation hydrofoil," *Journal of Shanghai Jiaotong University*, vol. 47, no. 6, pp. 878–883, 2013.

[3] S. Singh, M. Danish, and K. Saha, "Computational investigation of cavitating flow around two dimensional NACA 4424 and MHKF-240 hydrofoil," *Vibroengineering Procedia*, vol. 29, pp. 159–164, 2019.

[4] W. Wang, *Theoretical and Experimental Research on Unsteady Cavitation Suppression Around Hydrofoil*, Dalian University of Technology, Dalian, China, 2019.

[5] Y. Cheng, *Research on Cavitation Flow Based on OpenFOAM*, Harbin Institute of Technology, Harbin, China, 2014.

[6] W. Wang, *Research on Cavitation Flow Control of Centrifugal Pump with Low Specific Speed*, Jiangsu University, Zhenjiang, China, 2016.

[7] T. Sun, H. Chen, B. Zhu et al., "Optimal design of slotted impeller," *Journal of Shanghai University (Natural Science Edition)*, vol. 20, no. 2, pp. 207–213, 2014.

[8] h. Chen, y. Lin, and b. Zhu, "Experimental research on cavitation of centrifugal pump with slotted impeller," *Journal of Irrigation and Drainage Mechanical Engineering*, vol. 31, no. 7, pp. 570–574, 2013.

[9] W. Shi, J. Zhang, D. Zhang, R. Zhao, and L. Zhang, "Numerical simulation of cavitation characteristics of accelerated flow around hydrofoil," *Journal of Agricultural Machinery*, vol. 47, no. 4, pp. 1–7, 2016.

[10] W. Shi, Y. Shi, X. Gao, D. Zhang, and T. Lang, "Zhao simulation and experiment on flow characteristics of large particles in vortex pump based on DEM CFD," *Transactions of the Chinese Society for Agricultural Machinery*, vol. 51, no. 10, pp. 176–185, 2020.

[11] T. Hou, *Experimental Research on Cavitation Suppression Based on Active Control Technology*, Dalian University of Technology, Dalian, China, 2018.

[12] Y. Li, J. Wang, J. Wang, and Y. Zhang, "Numerical simulation of two-dimensional hydrofoil cavitation flow," *Chemical Machinery*, vol. 45, no. 2, pp. 261–266, 2018.

[13] W. Shi, Y. Zhang, Y. Xiao, and L. Zhou, "Research status of pump hydraulic design methods," *Journal of Nantong University (Natural Science Edition)*, vol. 18, no. 4, pp. 1–7, 2019.

[14] F. Numachi, "Aerofoil theory of propeller turbines and propeller pumps with special reference to the effects of blade interference upon the lift and the cavitation," *Journal of the Society of Mechanical Engineers*, vol. 31, no. 136, pp. 530–583, 2017.

[15] D.-d. Yang, Y. An, B. Ji et al., "Numerical analyses of ventilated cavitation over a 2-D NACA0015 hydrofoil using two turbulence modeling methods," *Journal of Hydrodynamics*, vol. 30, no. 2, pp. 345–356, 2018.

[16] M. Ghorbani, "Numerical study of cavitating flow in orifices and its effect on spray characteristics," *Journal of Hydrodynamics*, vol. 30, no. 5, pp. 908–919, 2018.

[17] Y. Zhang, J. Zhang, X. Lin et al., "Experimental investigation into downstream field of a horizontal axis tidal stream turbine supported by a mono pile," *Applied Ocean Research*, vol. 101, p. 102257, 2020.

[18] H. Ganesh, A. Bhatt, J. Wu et al., "Effect of compressibility on bubbly cavitating flows," *Journal of Hydrodynamics*, vol. 32, no. 7, pp. 1–5, 2020.

[19] Y. Zhang, E. Fernandez-Rodriguez, J. Zheng et al., "A review on numerical development of tidal stream turbine performance and wake prediction," *IEEE Access*, vol. 99, Article ID 2989344, 2020.

[20] J. Hu, X. Hou, and Y. Yu, "Improvement of Schnerr-Sauer cavitation model based on local flow characteristics," *Journal of Beijing Institute of Technology*, vol. 40, no. 3, pp. 1–8, 2020.

[21] F. Hong, Z. Gao, and J. Yuan, "Improvement and application of cavitation model based on Rayleigh-Plesset equation," *Journal of Agricultural Machinery*, vol. 49, no. 2, pp. 126–132, 2018.

[22] F. Hong, J. Yuan, B. Zhou et al., "Evaluation and analysis of improved Schnerr-Sauer model in hydrofoil cavitation simulation," *Journal of Harbin Engineering University*, vol. 37, no. 7, pp. 885–890, 2016.

[23] Z.-s. Xie, Y. Zheng, W.-d. Shi et al., "Investigation on the failure analysis of crimped composite insulators used in "V" type string," *Engineering Failure Analysis*, vol. 94, pp. 274–284, 2018.

[24] X. Sun, J. Liu, L. Ji et al., "A review on hydrodynamic cavitation disinfection: the current state of knowledge," *Science of the Total Environment*, vol. 737, p. 139606, 2020.